Domain Structure and Molecular Conformation in Annexin V/1,2-Dimyristoyl-*sn*-Glycero-3-Phosphate/Ca^{2+} Aqueous Monolayers: A Brewster Angle Microscopy/Infrared Reflection-Absorption Spectroscopy Study

Fangjun Wu,* Arne Gericke,# Carol R. Flach,* Tanya R. Mealy,§ Barbara A. Seaton,§ and Richard Mendelsohn*
*Department of Chemistry, Newark College of Arts and Science, Rutgers University, Newark, New Jersey 07102 USA; #Institut für Physikalische Chemie, Martin-Luther Universität Halle, Wittenberg 06108 Halle, Germany; and §Department of Physiology, Boston University School of Medicine, Boston, Massachusetts 02118 USA

ABSTRACT Annexins comprise a family of proteins that exhibit a Ca^{2+}-dependent binding to phospholipid membranes that is possibly relevant to their in vivo function. Although substantial structural information about the ternary (protein/lipid/Ca^{2+}) interaction in bulk phases has been derived from a variety of techniques, little is known about the temporal and spatial organization of ternary monolayer films. The effect of Ca^{2+} on the interactions between annexin V (AxV) and anionic DMPA monolayers was therefore investigated using three complementary approaches: surface pressure measurements, infrared reflection-absorption spectroscopy (IRRAS), and Brewster angle microscopy (BAM). In the absence of Ca^{2+}, the injection of AxV into an aqueous subphase beneath a DMPA monolayer initially in a liquid expanded phase produced BAM images revealing domains of protein presumably surrounded by liquid-expanded lipid. The protein-rich areas expanded with time, resulting in reduction of the area available to the DMPA and, eventually, in the formation of condensed lipid domains in spatial regions separate from the protein film. There was thus no evidence for a specific binary AxV/lipid interaction. In contrast, injection of AxV/Ca^{2+} at a total Ca^{2+} concentration of 10 μM beneath a DMPA monolayer revealed no pure protein domains, but rather the slow formation of pinhead structures. This was followed by slow (>2 h) rigidification of the whole film accompanied by an increase in surface pressure, and connection of solid domains to form a structure resembling strings of pearls. These changes were characteristic of this specific ternary interaction. Acyl chain conformational order of the DMPA, as measured by $\nu_{sym}CH_2$ near 2850 cm^{-1}, was increased in both the AxV/DMPA and AxV/DMPA/Ca^{2+} monolayers compared to either DMPA monolayers alone or in the presence of Ca^{2+}. The utility of the combined structural and temporal information derived from these three complementary techniques for the study of monolayers in situ at the air/water interface is evident from this work.

INTRODUCTION

Annexins comprise a family of eukaryotic proteins that bind to phospholipid membranes in a Ca^{2+}-dependent manner (for reviews, see Moss, 1992; Raynal and Pollard, 1994; Swairjo and Seaton, 1994; Seaton, 1996; Benz and Hofmann, 1997). The proteins have been implicated in a wide variety of cellular processes, including membrane trafficking and signal transduction. The calcium-dependent membrane binding is thought to play a central role in the cellular function of annexins, and thus a molecular understanding of this process is an important goal.

AxV is one of the most broadly distributed and abundant members of its family and has been widely studied in terms of structure and membrane interactions. The affinity of the protein for acidic phospholipid membranes is in the nanomolar range (Tait et al., 1989; Andree et al., 1990) in the presence of calcium, but can be reversed readily in model membrane systems by the addition of a calcium chelator such as EGTA. Combined evidence from various approaches supports a peripheral mode of membrane binding for AxV. Spectroscopic and other biophysical measurements, including surface pressure (Mukhopadhyay and Cho, 1996) and ellipsometry (Andree et al., 1990), rule out significant insertion of the protein into the lipid bilayer.

AxV is a 33-kDa polypeptide composed primarily of α-helical structure. The molecule contains four canonical domains of ~70 residues that are organized in a planar cyclical array. Most of the helices occur in α-helical bundles that lie perpendicular to the plane of the membrane. Structural data show that interhelical loops on the interfacial protein surface contain numerous calcium binding sites (Huber et al., 1990; Concha et al., 1993). Formation of the ternary complex involves interactions between protein atoms, calcium ions, and polar phospholipid moieties, including the phosphoryl oxygens (Meers and Mealy, 1994; Swairjo et al., 1994, 1995). Membrane-bound AxV can aggregate into ordered arrays along the membrane surface (Concha et al., 1992; Pigault et al., 1994), behavior thought to be of functional relevance. The effects of AxV binding on membrane structure and physical properties is thus of considerable interest. In a more general sense, the annexins may be a useful paradigm for understanding the association of

Received for publication 11 December 1997 and in final form 4 March 1998.

Address reprint requests to Dr. R. Mendelsohn, Department of Chemistry, Rutgers University, Newark College, 73 Warren Street, Newark, NJ 07102. Tel.: 973-353-5613; Fax: 973-353-1264; E-mail: mendelsohn@hades.rutgers.edu.

0006-3495/98/06/3273/09 $2.00

other peripheral membrane proteins with phospholipid assemblies.

The complexity of biological membrane surfaces warrants the use of model membrane systems to investigate interactions between peripheral membrane proteins and phospholipids. Model systems constructed from monolayers rather than vesicles (bilayers) offer greater control over experimental variables such as surface density, surface pressure, subphase composition, and molecular area. Although the early years of monolayer research relied primarily on pressure-area (π-A) isotherm determination for film characterization, several techniques have recently been developed that permit the direct determination of structural and morphological properties of monolayers at the air/water (A/W) interface. These are, most notably, x-ray reflection spectroscopy (Möhwald, 1990), epifluorescence (McConnell, 1991; Stine, 1994) and Brewster angle microscopies (BAM) (Vollhardt, 1996), and infrared reflection-absorption spectroscopy (IRRAS) (Mendelsohn et al., 1995). The last two of these methods, BAM and IRRAS, are based on similar physical principles, i.e., reflectivity differences between a bare water surface and a monolayer-covered surface. The two techniques provide characterization of monolayers at different distance scales. BAM experiments utilize a polarized visible laser to provide optical images of monolayers with a spatial resolution on the order of microns. The beam impinges on the surface at the Brewster angle for water, resulting in minimum reflectivity for p-polarized radiation (Hénon and Meunier, 1991; Hönig and Möbius, 1991). The presence of a monolayer alters the optical properties of the interface, resulting in enhanced reflectivity in film-covered regions, and thus permits domains to be visualized with an appropriate detector. IRRAS measurements provide structural information at the level of molecular functional groups, including estimates of acyl chain conformation. The information is a spatial average over the beam area (Flach et al., 1996; Cornut et al., 1996; Gericke et al., 1996). Structural data are inferred from the observed wavenumber positions, and orientational parameters are derived from the dependence of the reflected intensities of the polarized light components on the angle of incidence (Flach et al., 1997).

The current study reports a combined BAM/IRRAS/pressure-area isotherm investigation of AxV/dimyristoylphosphatidic acid (DMPA)/Ca^{2+} interaction. The results demonstrate the wide range of morphologies available to the interacting components and clearly reveal the importance of integrating the results from a variety of surface measurements to acquire a detailed picture of domain and molecular structure at the A/W interface.

MATERIALS AND METHODS

The monosodium salt of 1,2-dimyristoyl-*sn*-glycero-3-phosphate (DMPA) was purchased from Avanti Polar Lipids (Alabaster, AL). High-performance liquid chromatography grade H_2O, chloroform, and methanol were obtained from Fisher Scientific (Pittsburgh, PA). Deuterium oxide (D_2O) with 99.9% isotopic enrichment was purchased from Isotec (Miamisburg, OH). All other chemicals were obtained from Sigma (St. Louis, MO) and were of the highest purity commercially available.

Preparation of samples for BAM and IRRAS measurements

DMPA powder was dissolved in $CHCl_3$ to make a stock solution of 1.18 mg/ml. A subphase of 0.1 M NaCl and 2 mM ethylenediamine tetraacetate disodium salt (EDTA) in high performance liquid chromatography grade H_2O (pH 5.6) was used for all of the monolayer experiments. Recombinant rat AxV was prepared as described previously (Swairjo et al., 1994). AxV samples are stored in buffer A (50 mM HEPES, 100 mM KCl, 0.02% NaN_3, and 50 μM EGTA, pH 7.4) at 4°C. Protein concentration was determined by the Bradford assay. All experiments involving lipid and protein components had a maximum protein/lipid mole ratio of 1:5. The actual ratio in the monolayer is depends upon the extent of AxV adsorption. Ca^{2+}-free AxV samples were prepared by diluting 24.8 μl of a 6.4 mg/ml protein stock solution to 150 μl with buffer A. The AxV-Ca^{2+} samples were made by adding 9.1 μl of a 0.1 M Ca^{2+} solution to 24.8 μl of a protein stock solution and were diluted afterward with buffer A to comprise a total volume of 150 μl. The Ca^{2+} samples for control experiments were prepared by diluting 9.1 μl of 0.1 M Ca^{2+} with buffer A to yield 150 μl of solution. All protein samples were incubated at room temperature for 30 min before injection.

BAM imaging of the DMPA π-A isotherm

A Nima Technology (Coventry, England) 601M Langmuir-Blodgett trough equipped with a model PS-4 tensiometer was used for DMPA pressure-area isotherm measurements. The temperature of the subphase was controlled at 21.0 ± 0.5°C. The DMPA stock solution (7.6 μl) was spread with a Hamilton (Reno, NE) 10-μl micro syringe, yielding an area of 1.09 nm^2/molecule. After an initial relaxation period of 30 min, the film was compressed continuously at a speed of 2.27×10^{-2} nm^2/(molecule·min). If not otherwise indicated, this speed was utilized for all measurements.

An NFT (Göttingen, Germany) MiniBAM was aligned perpendicular to the compression direction. The polarizer and analyzer were set to p-polarization, and the incoming laser light (688 nm, 30 mW) was limited to an angle of incidence of 52–54° (Brewster angle for aqueous subphases). Images captured by a low geometrical distortion, sensitive, black/white frame transfer CCD camera were transferred in real time to a computer using a Univision (Burlington, MA) Scorpion 8G frame grabber card. The images were acquired and analyzed with the Image-Pro Plus 2.1 software (Media Cybernetics, Silver Spring, MD). BAM images were acquired in 1-min intervals and were cut to the desired size; no other manipulations were made.

BAM imaging of annexin V-DMPA

A DMPA monolayer was compressed to the onset of the LE/LC transition region (~0.70 nm^2/molecule). After a relaxation time of 10 min, 96.0 μl of sample was injected beneath the monolayer, using a 100-μl long-needle Hamilton microsyringe. AxV-Ca^{2+}, Ca^{2+}-free AxV, Ca^{2+}, and buffer A were used as required for the different experiments. BAM images and surface pressures were recorded as a function of time after injection. Typically, the overall running time of each postinjection experiment spanned 4–5 h.

IRRAS measurements

The experimental setup has been described in detail elsewhere (Flach et al., 1997). Briefly, the angle of incidence was set at 35°, and unpolarized radiation was used. A total of 1024 scans acquired with a resolution of 4 cm^{-1} were coadded and fast-Fourier transformed with one level of zero filling to yield spectra encoded every 2 cm^{-1}. The monolayer was discon-

tinuously compressed over a time period of 3 h. After reaching the LE/LC transition region, the monolayer was allowed to relax for at least 10 min before sample injection. The acquisition time for one spectrum was ~8 min. Band positions of the lipid methylene stretching vibrations were determined with a center-of-gravity algorithm, using software provided by the National Research Council of Canada.

RESULTS

In Fig. 1 the π/A isotherm for a pure DMPA ($T = 21°C$) monolayer is shown, and is in good agreement with data previously reported (Helm et al., 1987). In Fig. 2, the corresponding BAM images are displayed for those areas per molecule marked by the arrows in Fig. 1. In Fig. 2, *a–c*, are images representing the end of the gaseous/liquid-expanded (G/LE) coexistence region over a very small range of molecular areas. In Fig. 2 *a*, a fine, foamlike structure of LE domains in a gaseous ambient environment is discernible, which becomes increasingly dense (Fig. 2 *b*) and finally forms a homogeneous, brighter LE phase (*bottom left* in Fig. 2 *c*). Upon further compression, the monolayer reaches the LE/liquid-condensed (LC) phase transition, which is marked by the occurrence of predominantly circular condensed domains (Fig. 2 *d*), which increase in size and number with decreasing area per molecule (Fig. 2, *e* and *f*). Fig. 2 *g* displays a stripe, at the lower right (which was truncated during production of this figure), of dendritic-shaped domains floating through the field of view, indicating a nonequilibrium state of the monolayer (Gehlert and Vollhardt, 1997). In Fig. 2 *h* a nearly homogeneous LC phase is visible, whereas further compression to a surface pressure above the LC/Solid phase transition yielded a homogeneous grey-white image (not shown). These images are markedly different from those obtained in the presence of Ca^{2+}. Generally, the presence of moderate concentrations of Ca^{2+} resulted in nearly complete elimination of the plateau region in the π/A isotherm and in the formation of condensed domains, even at large areas per molecule (not shown).

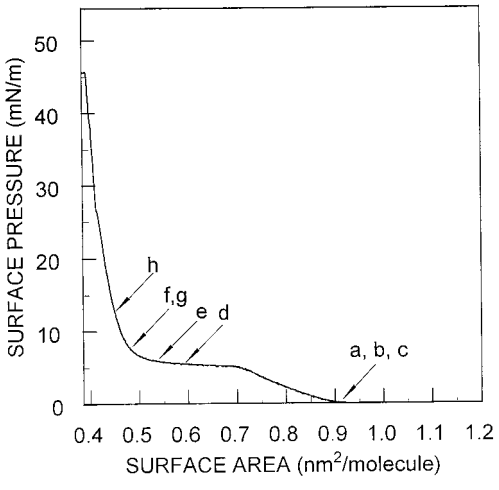

FIGURE 1 π/A isotherm ($T = 21°C$) of DMPA monolayer on a 100 mM NaCl/2 μM EDTA subphase. The compression speed was 2.27×10^{-2} nm^2/(molecule · min).

For the current investigation, knowledge of the time dependence of surface pressure changes was of importance. Fig. 3 shows the temporal change in surface pressure for a DMPA monolayer compressed to the beginning of the LE/LC phase transition after injection of Ca^{2+} into the subphase (yielding a final concentration of ~1 mM). The surface pressure drops by ~5 mN/m in the first 120 min, resulting in a final pressure of ~0.5 mN/m. In contrast, when the monolayer is allowed to relax at the same area per molecule without the injection of Ca^{2+}, a much smaller decrease in the surface pressure (by 0.5 mN/m) is noted. Fig. 4 *a* shows a BAM image of a DMPA monolayer before the injection of Ca^{2+}. The monolayer is predominantly in the LE phase at an area of 0.7 nm^2/molecule, and no LC domains are discernible in this image. The presence of scattered liquid crystal domains on the surface cannot be ruled out, as the BAM apparatus samples only a small fraction of the available area. In this and all subsequent experiments, the monolayer was allowed to relax for at least 10 min before injection of Ca^{2+} ions. Approximately 60–70 min after the injection, condensed dendritic domains appear (Fig. 4 *b*), which grow in size (Fig. 4 *c*) until they connect (Fig. 4 *d*) to form a large network structure exceeding the field of view. At the same time, some fairly large surface areas appeared to be free of film-forming material. Dendritic or fractal-type shapes are mostly attributed to nonequilibrium structures caused by relatively high compression rates (Gehlert and Vollhardt, 1997). The unstable growth of these domains has been attributed to mass concentration gradients in the monolayers (Vollhardt et al., 1995).

To compare AxV binding to DMPA in the absence and presence of Ca^{2+} ions, the concentration of Ca^{2+} ions must be reduced to a level at which condensation of DMPA by Ca^{2+} becomes insignificant. For a Ca^{2+} concentration of 10 μM, the surface pressure was reduced by only 2.5 mN/m within the first 25 min and increased only slightly afterward. No domains were formed within the entire time range investigated (4–5 h). Therefore, this Ca^{2+} concentration and area per molecule were selected for the AxV binding studies.

Upon injection of an AxV/Ca^{2+} mixture, the surface pressure drops by ~2.5 mN/m in the first 15–25 min and increases slightly thereafter (Fig. 5) for an additional 1.5 h. Up to this point, the temporal change of the surface pressure parallels the behavior of the monolayer under which only Ca^{2+} ions were injected to a concentration of 10 μM. At ~2 h after the injection, however, the surface pressure begins to increase strongly. The onset time for this phenomenon is quite reproducible (±5 min) for our experimental conditions. Fig. 6 shows the corresponding BAM images. Fig. 6 *a* displays the image of the DMPA monolayer before injection of the AxV/Ca^{2+} mixture. No domains are visible. Approximately 30 min after the injection, very small domains appear (Fig. 6 *b*). These structures coexist with re-

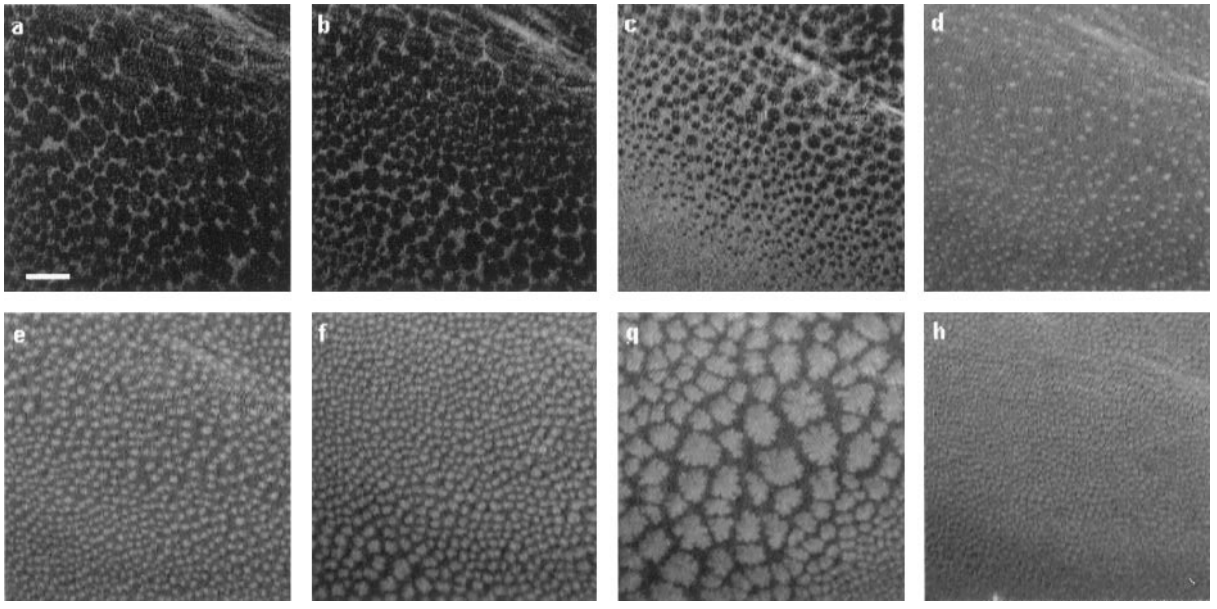

FIGURE 2 BAM images of a DMPA monolayer taken at the π/A values marked in Fig. 1. The images in *a–c* were acquired within 10 s, with dark areas representing gaseous regions and light areas the liquid expanded phase. In images *d–h*, bright areas represent regions of higher molecular density (domains). The scale bar in *a* represents 250 μm.

gions showing the same type of domains but at a higher density (Fig. 6 *c*), and with regions in which the domains are strongly enlarged and irregularly shaped (Fig. 6 *d*), whereas some regions are free of any domains. In the time following, the surface becomes increasingly covered with domains, and the whole film structure rigidifies. Near the time where the surface pressure starts to increase (Fig. 5, *e* and *f*), the small domains appear to be embedded in a more rigid condensed film structure (Fig. 6, *e* and *f*). Approximately 3 h after injection, the surface pressure is clearly increased

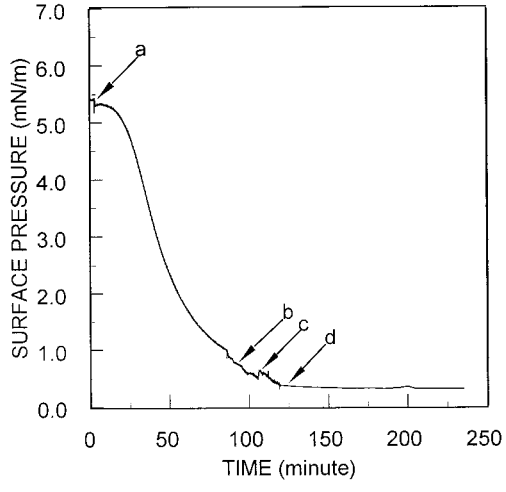

FIGURE 3 Surface pressure versus time after the injection of 96 μl 0.6 M Ca^{2+} (final concentration $\approx$ 1 mM) beneath a DMPA monolayer at an area of 0.7 nm^2/molecule (onset of the LE/LC transition region). The monolayer was compressed with a speed of 2.27×10^{-2} nm^2/(molecule · min) and was allowed to relax for 10 min before injection. Time 0 is the time of injection.

and the pinhead domains appear to associate into a striped, somewhat more connected structure. The contrast and focus of the image degraded slightly from this point, and it proved impossible to significantly improve the quality of the image. In particular, the deteriorating focus in Fig. 6, *e–h*, might suggest that the pinhead-type solid domains are associated with structures extending into the subphase. Upon completion of the experiment, it was noted that the monolayer was extremely rigid. It is further noted that the domains found for the AxV/Ca^{2+} experiment were distinctly different from those found when only Ca^{2+} ions were present.

The injection of protein alone below a surface covered with DMPA yielded an increase in surface pressure (Fig. 7). The corresponding BAM images are shown in Fig. 8, *a–f*. Shortly after injection, a diffuse increase in brightness was found. These large areas of increased brightness revealed structures of higher density (Fig. 8, *a* and *b*), probably arising from protein that was surrounded by liquid-expanded lipid phases. The protein-rich areas continued to grow, resulting initially in a reduction of the area available to the lipid molecules and eventually in the formation of condensed domains (Fig. 8, *c–f*). The fluidity of the lipid phase appeared to be considerably higher than of the protein phase, because the flow of the condensed domains in the lipid-rich phase was much faster than any movement associated with the protein-rich phase. Injection of greater amounts of AxV resulted in the formation of either larger lipid domains or protein-rich domains with distorted circular shapes, evolving in later stages into kidney-shaped domains (Fig. 8, *g* and *h*).

It is again emphasized that at all times, the morphological structure of the monolayer in the Ca^{2+}-free case was strik-

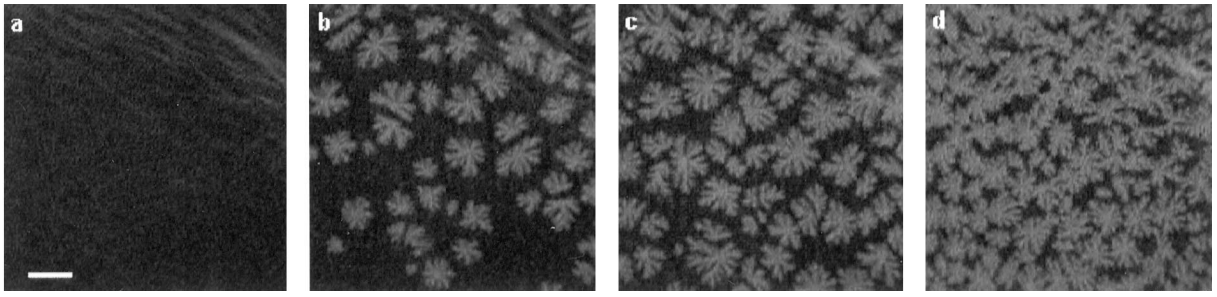

FIGURE 4 BAM images of a DMPA monolayer upon Ca^{2+} injection into the subphase, taken at the π/time values marked in Fig. 3. The image in *a* was captured just before the injection at an area of 0.7 nm^2/molecule (onset of LE/LC transition region). The bar in *a* represents 250 μm.

ingly different from the structure found in the presence of Ca^{2+}. In the absence of Ca^{2+}, AxV does not show a strong interaction with the lipid molecules. The condensation of the DMPA appears to be caused simply by the reduction of the available area due to protein adsorption. Furthermore, the protein- and lipid-rich areas appeared to be immiscible. In contrast, in the presence of Ca^{2+}, diffuse adsorption of the AxV was not observed. Condensation of the DMPA monolayer in the ternary system appears to be caused by the formation of a specific DMPA/AxV/Ca^{2+} structure.

To investigate the influence of AxV on lipid acyl chain order, the protein was injected into the subphase in the absence and presence of Ca^{2+}, and IRRAS measurements were performed. The DMPA symmetric CH_2 stretching frequencies were monitored as a function of time (Fig. 9). It is noted that for the BAM and IRRAS experiments, troughs with the same rectangular dimension but different depths were used, and the altered geometries in the two cases will influence the details of the adsorption kinetics. The temporal behavior of the $\nu_s(CH_2)$ frequency after AxV injection is unaltered by the presence of Ca^{2+}. IRRAS band positions show some scatter in the first 50 min, possibly caused by the fact that different domains float into and out of the beam area. In the following 100 min, the frequency decreases by $\sim$1.5 cm^{-1}, indicating that the acyl chains of the lipid molecules become increasingly ordered, reaching a level that is comparable to the conformational order of a pure DMPA monolayer in either a bulk gel or a monolayer solid phase. These data are in contrast to those obtained when Ca^{2+} alone was injected into the subphase. In this instance, a much smaller change in the frequency of the $\nu_s(CH_2)$ band was observed with time. The acyl chains in this film were therefore more disordered than in the protein-containing films. The conformational ordering observed in Fig. 9 is evidently caused by the presence of the protein; however, no differences between Ca^{2+}-bound and free AxV can be inferred. The ordering of DMPA in the presence of pure AxV is most likely caused by the adsorption of protein to the interface, which reduces the available area per lipid molecule and drives the DMPA molecules through the LE/LC transition. The corresponding BAM images (Fig. 8) show the development of large protein domains with an undefined shape and the formation of apparently pure DMPA condensed domains. In contrast, the injection of AxV/Ca^{2+} resulted in a completely different domain structure (Fig. 6) and revealed a direct interaction between AxV/Ca^{2+} and DMPA. However, the conformational ordering of the DMPA molecules caused by this interaction cannot be distinguished by IRRAS from the ordering, because of the reduction of the available area as a result of protein adsorption. This inability of IRRAS to distinguish a strong interaction from a situation in which the protein merely occupies the surface is true for both the absolute frequency values approached by $\nu_s(CH_2)$ as equilibrium is achieved, as well as for the temporal dependence of the frequency change after injection. Whereas for the pure AxV case it is quite obvious that the protein penetrates to the monolayer surface without a direct interaction with the DMPA molecules, it is less clear from the BAM images whether the AxV/Ca^{2+} penetrates the monolayer or interacts solely with the headgroups of the DMPA molecules. Because the DMPA monolayer becomes highly condensed in the presence of AxV/

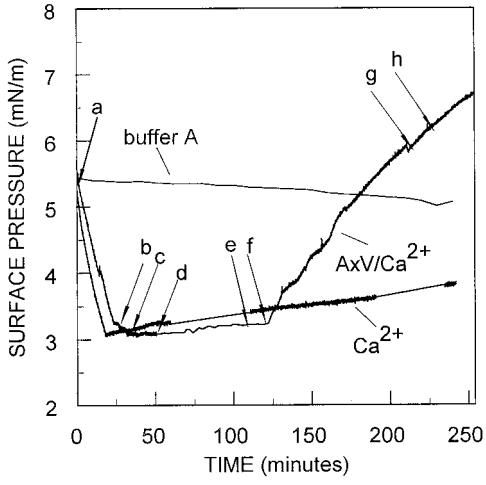

FIGURE 5 Surface pressure versus time after injection of AxV/Ca^{2+} (final protein concentration $\approx$ 0.06 μM, final Ca^{2+} concentration $\approx$ 10 μM, and DMPA/AxV molar ratio $\approx$ 5:1), Ca^{2+} (final concentration $\approx$ 10 μM), and buffer A beneath a DMPA monolayer at an area of 0.7 nm^2/molecule (onset of LE/LC transition region). The monolayer was compressed with a speed of 2.27 $\times$ 10^{-2} nm^2/(molecule $\cdot$ min) and was allowed to relax for 10 min before injection. Points *a–h* correspond to points where BAM images were taken. The BAM images are shown in Fig. 6.

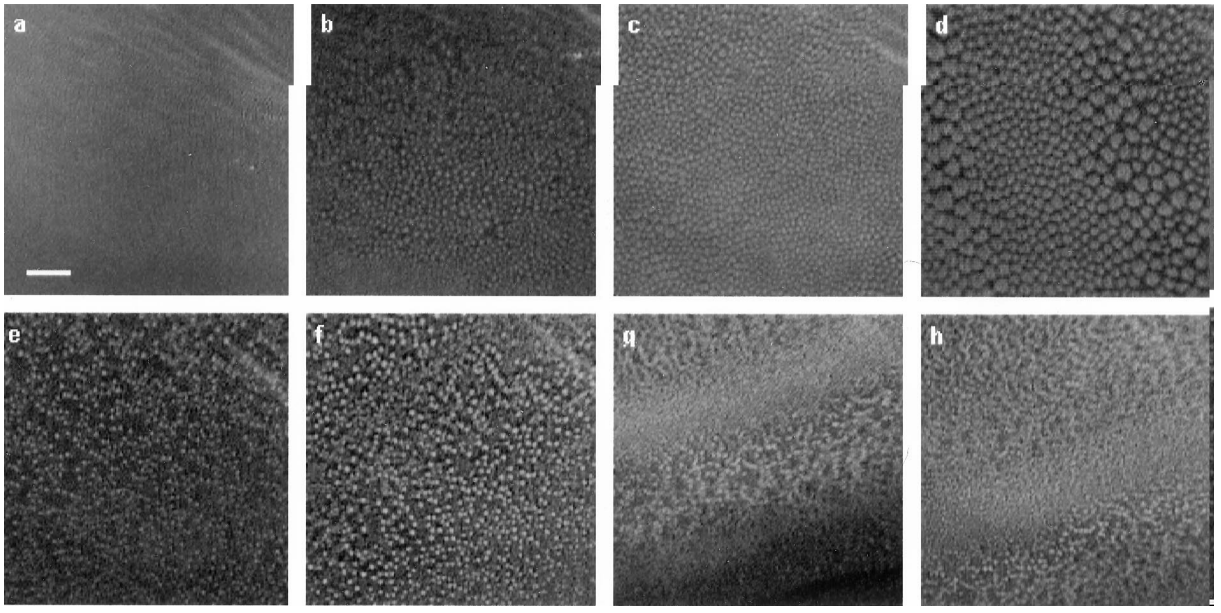

FIGURE 6 BAM images of a DMPA monolayer in the presence of AxV/Ca^{2+} taken at the π/time values marked in Fig. 5. Image *a* was taken just before the injection beneath a DMPA monolayer at an area of 0.7 nm^2/molecule (onset of LE/LC transition region). The scale bar in *a* represents 250 μm.

Ca^{2+} and the conformational order of the DMPA molecules increases upon interaction, it is very unlikely that the protein inserts into the lipid monolayer domains. Insertion into ordered domains would induce a distortion of the lipid monolayer structure, probably accompanied by disordering of the lipid acyl chains. As neither of these phenomena occurs, it is concluded on the basis of the BAM images and the IRRAS measurements that the AxV/Ca^{2+} interacts with the DMPA headgroups.

DISCUSSION

In the current study, the images provided by BAM, supplemented with the kinetic and molecular structural data provided by surface pressure and IRRAS measurements, respectively, offer a unique set of tools for monitoring the spatial and temporal organization of both the proteins and lipids in monolayer films. Data from the BAM experiments support the current model that describes the calcium-dependent binding AxV to membrane surfaces in bulk phases. The presence of DMPA monolayers, along with 10 μM Ca^{2+} levels in the subphase, is shown in the current work to promote specific interactions between AxV and the phospholipid aggregates that are lacking in the absence of either the cation or the lipid. High-resolution images from cryo-electron microscopy AxV on phospholipid monolayers (Voges et al., 1994; Olofsson et al., 1994) show that membrane-bound AxV maintains a structure that is similar to the x-ray crystal structure, except for a slight flattening of the molecule on the membrane surface. Circular dichroism spectra of AxV in the presence or absence of calcium and acidic phospholipid vesicles have shown no substantive differences (Swairjo et al., 1994; Sopkova et al., 1994).

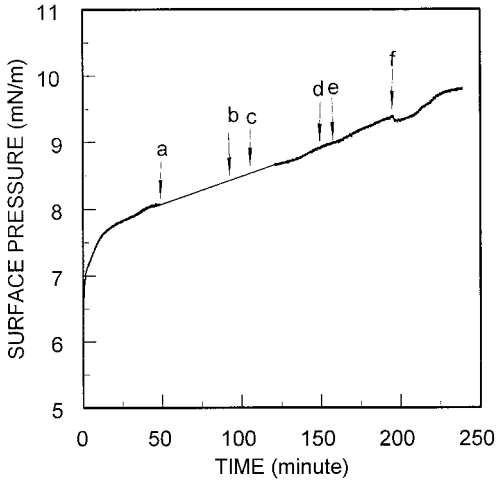

FIGURE 7 Surface pressure versus time after injection of AxV beneath a DMPA monolayer at an area of 0.7 nm^2/molecule (onset of LE/LC transition region, final protein concentration $\approx$ 0.06 μM, $T = 21 \pm 0.5$°C). The subphase contains 100 mM NaCl and 2 μM EDTA.

Significant dynamic changes occur in the DMPA monolayer when the ternary Ax/Ca^{2+}/DMPA complex forms. The surface pressure drops precipitously in the first few minutes after calcium addition, independent of the presence of AxV (Figs. 3 and 5). However, only in the presence of protein does a substantial increase in surface pressure appear after a lag period of ~2 h. The reorganization in domain structure that occurs in this time regime (Fig. 6, *g* and *h*) is pronounced. The striking horizontal swaths appear diffuse as the image becomes defocused in these areas. The loss of focus suggests that the geometry and thickness of the film are affected by the molecular aggregation associated with ternary complex formation. The slow time course for these effects is notable, because the kinetics of AxV binding to large planar membranes is diffusion limited (Andree et

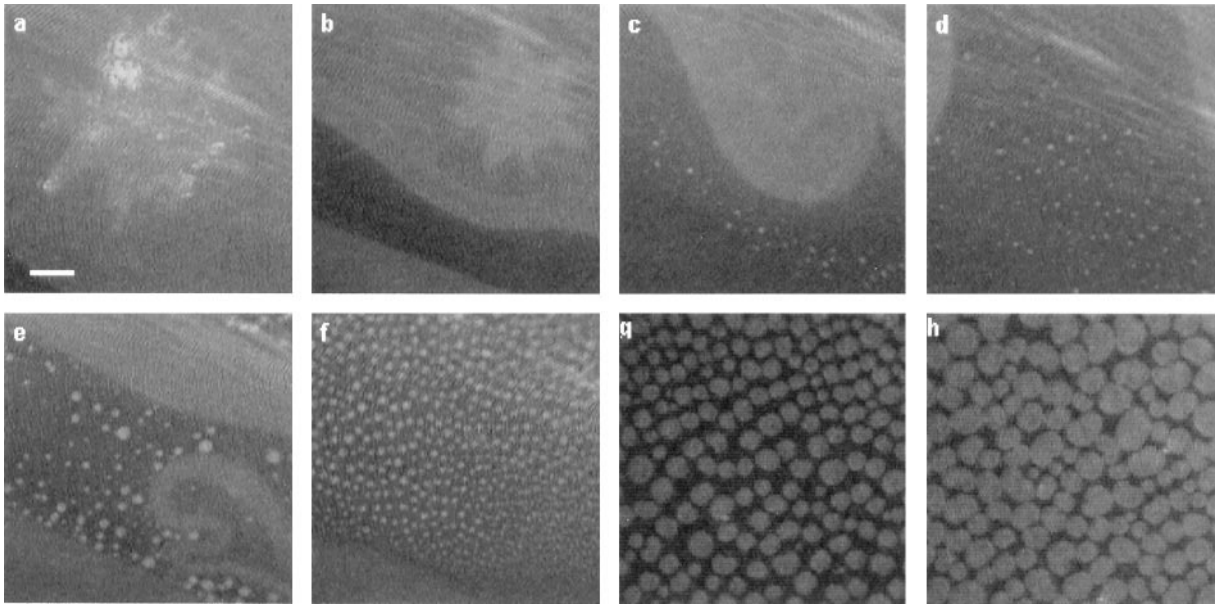

FIGURE 8 (*a–f*) BAM images of a DMPA monolayer in the presence of AxV (final concentration ≈ 0.06 μM) taken at π/time values marked in Fig. 7. The monolayer was compressed to 0.7 nm^2/molecule (onset of LE/LC transition region) with a speed of 2.27×10^{-2} nm^2/(molecule · min). *g* and *h* are from a separate experiment. They represent images taken 160 min after injection of AxV (final concentration ≈ 0.6 μM) beneath a DMPA monolayer. The same protocol was followed by DMPA monolayer.

al., 1990). Clearly, the major domain reorganizations implied in the surface pressure/time data (Fig. 5) and visualized in the BAM images require significant time to be established.

The BAM images permit direct visualization at a resolution of 10–20 μm of several annexin-induced alterations in bilayer properties. Results from several bulk-phase spectroscopic studies (Meers et al., 1991; Junker and Crentz, 1993; Sobota et al., 1993; Gilmanshin et al., 1994) have found that the binding of annexins IV–VI to membranes reduces lipid lateral mobility and membrane fluidity. In mixed lipid vesicle systems, calcium-dependent binding of annexins leads to clustering of acidic phospholipids (Bazzi and Nelsestuen, 1992). Similarly, clustering or self-association of protein molecules also takes place on membrane surfaces (Zaks and Creutz, 1991; Concha et al., 1992). The competition for membrane surface area by segregated annexin at the expense of pure lipid microdomains has been suggested as the basis for annexin inhibition of thrombin and phospholipase A2 (Davidson et al., 1987; Andree et al., 1992), as these enzymes require phospholipid membrane docking sites for function. The BAM images in Figs. 6 and 9 demonstrate the ability of the protein to either associate directly with acidic lipids in a calcium-dependent manner in a monolayer (Fig. 6), or to compete for monolayer surface area, even in the absence of calcium (Fig. 8).

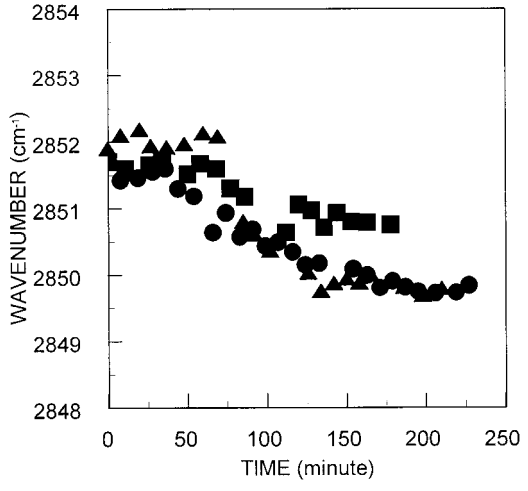

FIGURE 9 Frequencies of the $\nu_s(CH_2)$ vibration for a DMPA monolayer ($T = 21 \pm 0.5$°C) versus time after the injection of AxV/Ca^{2+} (●), AxV (▲), as well as Ca^{2+} (■) into a 100 mM NaCl/2 μM EDTA subphase (final protein concentration ≈ 0.06 μM and final Ca^{2+} concentration ≈ 10 μM). The monolayer was compressed discontinuously to the onset of the LE/LC transition region.

Calcium-dependent annexin binding has been shown to stabilize the membrane, reducing leakiness and permeability to small molecules such as fura-2, a calcium indicator (Goossens et al., 1995). Studies of synthetic vesicle systems suggest that annexin binding and perhaps oligomerization reduce membrane curvature (Andree et al., 1992; Swairjo et al., 1994). The present studies reveal a strong conformational ordering of the lipid acyl chains in the ternary complex consistent with a structural rigidification. The acyl chains are also ordered by the simple presence of protein in the binary (calcium-free) film. The latter result may have no counterpart in lipid vesicles or native membranes, in which large changes in the area per lipid molecule, easy to affect

(by the simple adsorption of annexin) in monolayers, may be more difficult to induce.

The current suggestion that the AxV/Ca^{2+} interaction occurs with the lipid headgroups is similar to that found by Diederich et al. (1996) for the interaction of bacterial surface layer proteins with phosphatidylethanolamine monolayers. They showed by dual labeling fluorescence microscopy that the protein starts to nucleate at the boundary lines between the fluid and condensed lipid phases, and that crystallization proceeds beneath the condensed domains.

More generally, the complementary nature of the information from the three surface approaches utilized in the current work provides significant advantages for studying the interaction of peripheral membrane proteins with lipid monolayers. The time evolution of the surface pressure, a thermodynamic function, directly reveals the occurrence of the ternary interaction but provides no structural data. The BAM images provide domain size information down to $\sim$15 μm spatial resolution from both the lipid and protein components in the monolayer without the necessity for fluorophore incorporation, whereas the IRRAS data provide molecular-level information about the molecules in the domains. The methods all provide information about the slow approach to equilibrium in these monolayers.

RM and BAS were supported through grants from the Public Health Service (GM-29864 and GM-44554, respectively). AG received a fellowship from the Deutsche Forschungsgemeinschaft (DFG). We thank Prof. Ed Bonder for advice about the preparation of figures.

REFERENCES

Andree, H. A. M., C. P. M. Reutelingsperger, R. Hauptmann, H. C. Hemker, W. T. Hermens, and G. M. Willems. 1990. Binding of vascular anticoagulant alpha (VAC alpha) to planar phospholipid bilayers. *J. Biol. Chem.* 265:4923–4928.

Andree, H. A. M., M. C. A. Stuart, W. T. Hermens, C. P. M. Reutelingsperger, H. C. Hemker, P. M. Frederik, and G. M. Willems. 1992. Clustering of lipid-bound annexin V may explain its anticoagulant effect. *J. Biol. Chem.* 267:17907–17912.

Bazzi, M. D., and G. L. Nelsestuen. 1992. Interaction of annexin VI with membranes: highly restricted dissipation of clustered phospholipids in membranes containing phosphatidylethanolamine. *Biochemistry.* 31: 10406–10413.

Benz, J., and A. Hofmann. 1997. Annexins—from structure to function [Review]. *Biol. Chem.* 378:177–183.

Concha, N. O., J. F. Head, M. A. Kaetzel, J. R. Dedman, and B. A. Seaton. 1992. Annexin V forms calcium-dependent trimeric units on phospholipid vesicles. *FEBS Lett.* 314:159–162.

Concha, N. O., J. F. Head, M. A. Kaetzel, J. R. Dedman, and B. A. Seaton. 1993. Rat annexin V crystal structure: Ca^{2+}-induced conformational changes. *Science.* 261:1321–1324.

Cornut, I., B. Desbat, J. M. Turlet, and J. Dufourcq. 1996. In situ study by polarization modulation Fourier transform infrared spectroscopy of the structure and orientation of lipids and amphipathic peptides at the air/water interface. *Biophys. J.* 70:305–312.

Davidson, F. F., E. A. Dennis, M. Powell, and J. R. Glenney, Jr. 1987. Inhibition of phospholipase A_2 by lipocortins and calpactins—an effect of binding to substrate phospholipids. *J. Biol. Chem.* 262:1698–1705.

Diederich, A., C. Sponer, D. Pum, U. B. Sleytr, and M. Lösche. 1996. Reciprocal influence between the protein and lipid components of a lipid-protein membrane model. *Colloids Surfaces B.* 6:335–346.

Dieudonné, D., A. Gericke, C. R. Flach, X. Jiang, R. S. Farid, and R. Mendelsohn. 1998. Propensity for helix formation in the hydrophobic peptides K_2LA_x (x = 6, 8, 10, 12) in monolayer, bulk, and lipid-containing phases. Infrared and circular dichroism studies. *J. Am. Chem. Soc.* 120:792–799.

Flach, C. R., A. Gericke, and R. Mendelsohn. 1997. Quantitative determination of molecular chain tilt angles in monolayer films at the air/water interface—infrared reflection/absorption spectroscopy of behenic acid methyl ester. *J. Phys. Chem. B.* 101:58–65.

Flach, C. R., F. G. Prendergast, and R. Mendelsohn. 1996. Infrared reflection-absorption of melittin interaction with phospholipid monolayers at the air/water interface. *Biophys. J.* 70:539–546.

Gehlert, U., and D. Vollhardt. 1997. Nonequilibrium structures in 1-monopalmitoyl-*rac*-glycerol monolayers. *Langmuir.* 13:277–282.

Gericke, A., D. J. Moore, R. K. Erukulla, R. Bittman, and R. Mendelsohn. 1996. Partially deuterated phospholipids as IR structure probes of conformational order in bulk and monolayer phases. *J. Mol. Struct.* 379: 227–239.

Gilmanshin, R., C. E. Creutz, and L. K. Tamm. 1994. Annexin IV reduces the rate of lateral lipid diffision and changes the fluid phase structure of the lipid bilayer when it binds to negatively charged membranes in the presence of calcium. *Biochemistry.* 33:8225–8232.

Goossens, E. L. J., C. P. M. Reutelingsperger, F. H. M. Jongsma, R. Kraayenhof, and W. T. Hermens. 1995. Annexin V perturbs or stabilises phospholipid membranes in a calcium-dependent manner. *FEBS Lett.* 359:155–158.

Helm, C. A., H. Möwald, K. Kjaer, and J. Als-Nielsen. 1987. Phospholipid monolayers between fluid and solid states. *Biophys. J.* 52:381–390.

Hénon, S., and J. Meunier. 1991. Microscope at the Brewster angle. Direct observation of first order phase transitions in monolayers. *Rev. Sci. Instrum.* 62:936–939.

Hönig, D., and D. Möbius. 1991. Direct visualization of monolayers at the air/water interface by Brewster angle microscopy. *J. Phys. Chem.* 95: 4590–4592.

Huber, R., M. Schneider, I. Mayr, J. Römisch, and E. P. Pâques. 1990. The calcium binding sites in human annexin V by crystal structure analysis at 2.0 Å resolution. Implications for membrane binding and calcium channel activity. *FEBS Lett.* 275:15–21.

Junker, M., and C. E. Creutz. 1993. Endonexin (annexin IV)-mediated lateral segregation of phosphatidylglycerol in phosphatidylglycerol/phosphatidylcholine membranes. *Biochemistry.* 32:9968–9974.

McConnell, H. M. 1991. Structures in transitions in lipid monolayers at the air/water interface. *Annu. Rev. Phys. Chem.* 42:171–195.

Meers, P., D. Daleke, K. Hong, and D. Papahadjopoulos. 1991. Interactions of annexins with membrane phospholipids. *Biochemistry.* 30: 2903–2908.

Meers, P., and T. Mealy. 1994. Phospholipid determinants for annexin V binding sites and the role of tryptophan 187. *Biochemistry.* 33: 5829–5837.

Mendelsohn, R., J. W. Brauner, and A. Gericke. 1995. External infrared reflection absorption spectrometry monolayer films at the air-water interface. *Annu. Rev. Phys. Chem.* 46:305–334.

Möhwald, H. 1990. Phospholipid and phospholipid-protein monolayers at the air/water interface. *Annu. Rev. Phys. Chem.* 41:441–476.

Moss, S. E., editor. 1992. The Annexins. Portland Press, London.

Mukhopadhyay, S., and W. Cho. 1996. Interactions of annexin V with phospholipid monolayers. *Biochim. Biophys. Acta.* 1279:58–62.

Olofsson, A., V. Mallouh, and A. Brisson. 1994. Two-dimensional structure of membrane-bound annexin V at 8 Å resolution. *J. Struct. Biol.* 113:199–205.

Pigault, C., A. Follenius-Wund, M. Schmutz, J. M. Freyssinet, and A. Brisson. 1994. Formation of two-dimensional arrays of annexin V on phosphatidylserine-containing liposomes. *J. Mol. Biol.* 236:199–208.

Raynal, P., and H. B. Pollard. 1994. Annexins: the problem of assessing the biological role for a gene family of multifunctional calcium- and phospholipid-binding proteins. *Biochim. Biophys. Acta.* 1197:63–93.

Seaton, B. A., editor. 1996. Annexins: Molecular Structure to Cellular Function. R. G. Landes Co., Austin, TX.

Sobota, A., J. Bandorowicz, A. Jezierski, and A. F. Sikorski. 1993. The effect of annexin IV and VI on the fluidity of phosphatidylserine/phosphatidylcholine bilayers studied with the use of 5-deoxylstearate spin label. *FEBS Lett.* 315:178–182.

Sopkova, J., J. Gallay, M. Vincent, P. Pancoska, and A. Lewit-Bentley. 1994. The dynamic behavior of annexin V as a function of calcium ion binding: a circular dichroism, UV absorption, and steady-state and time-resolved fluorescence study. *Biochemistry.* 33:4490–4499.

Stine, K. J. 1994. Investigations of monolayers by fluorescence microscopy. *Microsc. Res. Tech.* 27:439–450.

Swairjo, M. A., N. O. Concha, M. A. Kaetzel, J. R. Dedman, and B. A. Seaton. 1995. Ca^{2+}-bridging mechanism and phospholipid head group recognition in the membrane-binding protein annexin V. *Nature Struct. Biol.* 2:968–974.

Swairjo, M. A., M. F. Roberts, M. B. Campos, J. R. Dedman, and B. A. Seaton. 1994. Annexin V binding to the outer leaflet of small unilamellar vesicles leads to altered inner-leaflet properties: ^{31}P- and ^{1}H-NMR studies. *Biochemistry.* 33:10944–10950.

Swairjo, M. A., and B. A. Seaton. 1994. Annexin structure and membrane interactions: a molecular perspective. *Annu. Rev. Biophys. Biomol. Struct.* 23:193–213.

Tait, J. F., D. Gibson, and K. Fujikawa. 1989. Phospholipid binding properties of human placental anticoagulant protein-I, a member of the lipocortin family. *J. Biol. Chem.* 264:7944–7949.

Voges, D., R. Berendes, A. Burger, P. Demange, W. Baumeister, and R. Huber. 1994. Three-dimensional structure of membrane-bound annexin V. A correlative electron microscopy–x-ray crystallography study. *J. Mol. Biol.* 238:199–213.

Vollhardt, D. 1996. Morphology and phase behaviour of monolayers. *Adv. Colloid Interface Sci.* 64:143–171.

Vollhardt, D., T. Gutberlet, G. Emrich, and J.-H. Fuhrhop. 1995. Dendritic crystal growth in *N*-dodecylgluconamide monolayers at the air/water interface. *Langmuir.* 11:2661–2668.

Zaks, W. J., and C. E. Creutz. 1991. Ca^{2+}-dependent annexin self-association on membrane surfaces. *Biochemistry.* 30:9607–9615.